8th International Conference on Water Resources and Arid Environments (ICWRAE 8): 256-269
22-24 January 2019*, Riyadh, Saudi Arabia*

Evaluation of METRIC for Estimation of Actual Evapotranspiration Using Satellite Imagery from Dryland Wheat Based Agricultural Systems in IPNW

[1]M. Azeem Khan, Claudio O. Stckle, [2]Richard G. Allen, [1]Jinshu Chi, [1]Eric S. Russell and [1]Ricardo Trezzab

[1]Washington State University, Pullman WA
[2]University of Idaho, Kimberly ID

Abstract: Evapotranspiration (ET) is the largest consumer of fresh water resources globally and spatio-temporal information on actual ET (ET_a) is important to ensure sustainable management of water resources. Surface energy balance applications based on satellite remote sensing can provide regional ET_a estimates with spatio-temporal variations. This study implemented the surface energy balance algorithm METRIC (Mapping Evapotranspiration at High resolution with Internalized Calibration) for use in the dryland farming region of the US Inland Pacific Northwest (IPNW). The study area had four eddy covariance flux towers deployed within a single scene setting of the Landsat 8 path 43 row 27, which allowed comparison with the ET_a estimated by METRIC. Estimated and measured daily ET_a showed a strong positive linear correlation with a Pearson's r value of 0.90 to 0.98 and a SEE ranging from 0.3 to 0.5 mm/day. The higher bias was generally associated with fallow periods. The Nash-Sutcliffe efficiency coefficient showed that METRIC is 82-98% efficient in estimating ET_a. These evaluations suggest that METRIC can estimate ET_a with good accuracy at regional scales in dryland areas where crops are often water limited.

Key words: Evapotranspiration · Surface Energy Balance · Water Stress · Remote Sensing · Drylands

INTRODUCTION

Evapotranspiration (ET) is the second largest term in the terrestrial water budget after precipitation and it is expected to increase with global warming [1]. Actual ET (ET_a) is a difficult component to assess, although a number of techniques are in use ranging from point measurements to modeling and to spatially-distributed remote sensing estimates [2]. Ground observations based on conventional methods including micrometeorological methods (e.g., , the Bowen ratio, eddy covariance), models (e.g., Penman–Monteith), weighing lysimeters and water balance methods (e.g., non-weighing lysimeters and field plots) are used for ET measurement at the individual plant and field scales [3]. Although these methods offer acceptable solutions for computing ET at a point/field scale over homogenous surfaces, extrapolation to larger spatial scales is not straightforward because of the natural variability in environmental and land surface conditions [4, 5]. Satellite remote sensing of surface fluxes at diverse spatial and temporal scales has emerged since the utility of the thermal infrared remote sensing was recognized [6-8]. ET is typically modeled using weather data and algorithms that describe surface energy and aerodynamic characteristics of the vegetation. In irrigated agriculture, plant density, height, vigor and water availability are normally homogeneous and measurement of ET and the application of estimation algorithms can be relatively straightforward, still not without substantial challenge [9, 10]. However, in drylands agriculture, the heterogeneous nature of vegetation, terrain, soils and water availability make aerodynamic processes and surface energy highly variable and poorly defined over large scales. The ground parameters, including vegetation types, elevation, terrain and land surface temperature have an obvious effect on spatial distribution of ET_a [11] and models cannot mimic that effect at regional scales without the use of spatial techniques and satellite images.

The primary benefit of spatial techniques is that ET_a from the pixel level (usually 30 m for Landsat satellite) to basin and regional scales can be estimated directly by using energy balance algorithms rather than by quantifying the other complex hydrological processes, which involve detailed information about soil-plant-atmosphere interaction at high spatial and temporal scale [12-14]. A number of surface energy balance algorithms

Corresponding Author: M. Azeem Khan, Washington State University, Pullman WA. E-mail: azeemwsu@gmail.com.

are used to estimate ET_a, that vary in mechanisms and degrees of complexity [15, 16]. Mapping Evapotranspiration at high Resolution with Internalized Calibration (METRIC), is so far one of the most appreciated surface energy balance algorithms for ET_a estimation [6, 10, 17-26]. METRIC estimates ET as the residual of the energy balance, by virtue of its inverse calibration technique METRIC has the ability to compensate for the biases in other components of the energy balance (e.g., Net Radiation and soil heat flux) and some components of the sensible heat flux calculations and therefore errors are reduced in ET_a estimates [18].

This study reports the results of the first multi-year remote sensing estimates of regional ET_a compared with Eddy Covariance (EC) measurements of water flux over the unique and highly productive dryland wheat cropping system of the Inland Pacific Northwest (IPNW). We analyze METRIC estimated ET_a over three sequential crop years at four sites with very different rainfall regimes in the IPNW.

The overall goal of this research is to evaluate METRIC regional ET_a estimation in dryland regions of the US IPNW. The study area included the dryland wheat-based cropping systems in eastern Washington, where a steep east to west precipitation gradient occurs and dryland farmers use a wide array of wheat (*Triticum aestivum* L.) based crop rotations, from continuous annual cropping (high rainfall, high yields) to wheat-fallow (low rainfall, low yields every other year), thereby producing varying amounts of crop residues and soil moisture patterns [27]. Though extensive studies of agro-ecosystems have been performed in this region [27, 28], this work is the first use of Landsat satellite imagery to estimate ET_a in dryland Washington.

MATERIALS AND METHODS

Study Area and Field Setup: The study sites are located in IPNW wheat-based cropping region, that extends from central Washington to eastern Washington and is covered by the single scene setting of the Landsat 8 OLI path 43 row 27. The EC measurements presented in this study were acquired for 2013, 2014 and 2015, from the Washington State University's Dryland Research stations in LIND and Pullman.EC flux towers are set up at four sites with contrasting characteristics in our study region (Table 1.). One site is located in LIND (center-east Washington) called LIND, two sites located in Pullman, (eastern Washington) called CFCT (Cook Farm Conventional Tillage), CFNT (Cook Farm No-Till)and one site located just outside Pullman, in Moscow, ID called MSMN (Moscow Mountain) (Fig. 1). All the EC flux tower systems installed at these sites have similar instrumentation set up, data collection and quality assurance procedures, they are deployed as part of the same project Regional Approaches to Climate Change (REACCH) USDA-supported research program (https://www.reacchpna.org/).The sites are in contiguous precipitation zones of this study region with average annual precipitation ranging from 240 to 680 mm (Fig. 1). Most of the annual precipitation ~ 70% is received during winter season [29, 30].

At CFCT, CFNT and MSMN the soils are silt loam (Mollisol)(Soil Survey Staff, N.R.C.S. and United States Department of Agriculture, 1999, 2013) with 2–5% organic matter in the top 20 cm [31]. The average high temperature is 26°C in the summer and the low is -4?C in the winter, with an overall average annual temperature of 9°C from1981–2010 [32]. At LIND the soils are silt loam (Mollisol), with 1–2% organic matter in the top 20 cm [33]. The average high and low temperatures are 30°C and -6° C, with an annual average of 10° C [34].The prevailing wind directions in the region are from the southwest and east. The wind-rose (Fig 1.) present the wind direction, speed and frequency at all the sites during our study period. CFNT and CFCT had spring garbanzo (Cicer Arietinum, "SG"), winter wheat (Triticum Aestivum L., "WW") and spring canola (SC) crops during the three growing seasons of our study respectively. MSMN had spring beans (SB), spring peas (SP) and WW during the study period. While LIND site had WW in 2013 and 2015 and it was fallow during 2014. In fallow period, the field was tilled to build up soil moisture in the seed-zone to increase productivity of the following WW crop.

Field Measurements: A brief overview of the filed setup of eddy covariance measurements is mentioned here. This data has been thoroughly examined and data from 2012 to 2013 has published in two separate studies [35, 36]. The eddy covariance (EC) instrumentation at each site consisted of an open-path infrared CO_2/H_2O analyzer and three-dimensional sonic anemometer (EC150/ CSAT3A/EC100, Campbell Scientific, Logan, UT, USA) at a height of~2.0 m. Data was collected at 10 Hz by a data logger (CR3000, Campbell Scientific, Logan, UT). Measurements used here were collected from March, 2013 to October, 2015. The final fluxes were calculated using EddyPro®version4.2.0 (LI-COR Biosciences, Lincoln, NE, USA). Data were processed via: spike detection and removal (Vickers and Mahrt, 1997), filtering by absolute limits and for CO^2 and H_2O signal strength below 80%. Double coordinate rotation was used [37]

Table 1: Summary of key characteristics of study region

Characteristics	CFCT	CFNT	LIND	MSMN
Avg annual precipitation	550 mm	550 mm	247 mm	680 mm
Location	46.78°N, 117.08°W	46.78°N, 117.09°W	46.99°N, 118.60°W	46.75°N, 116.95°W
Elevation	800 masl	800 masl	475 masl	815 masl
Avg annual temp	9°C	9°C	10°C	9°C
Tillage type	Chisel plow and cultivate	Direct drill (no-tillage)	Chisel plow and cultivate (reduced tillage)	Chisel plow and cultivate
Crop rotation	Continuous cropping	Continuous cropping	Crop-fallow	Continuous cropping

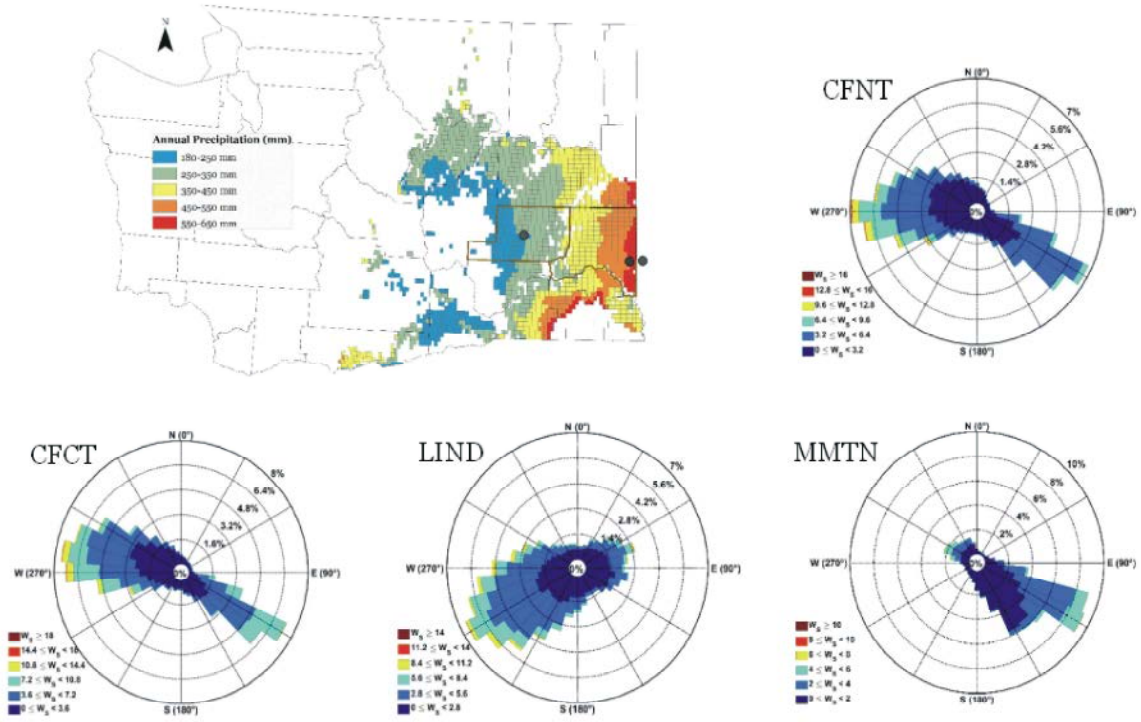

Fig. 1: Locations of study sites; Washington State IPNW with the long-term average annual precipitation variations information by location. The wind-roses present the dominant wind direction and frequencies at each site through our time period of study

as well as frequency loss corrections [38, 39] and the Webb, Pearman, Leuning(WPL) density correction [40]. The flux outputs were then filtered for remaining outliers using the procedure described in [41]. The flux datasets were gap filled using a combination of methods. First, gaps in the flux datasets due to loss of the raw10 Hz data were filled using fluxes calculated by the data logger operating program, where available. Remaining gaps in the ET, H and LE fluxes were filled using the mean diurnal variation (MDV) method [42, 43], which estimates a flux value for a missing half-hour period by averaging the values of adjacent days at that same time period. We used a time window of the ten days before and after a missing point for the MDV gap filling. For more detailed information on NLR and MDV gap-filling employed here[35]. However other than the missing data from 7th June to 18th July 2013, no data gaps were found for selected Landsat over-pass dates in this study.

In addition to EC measurement hourly and daily weather information was acquired from Washington State University's AgWeatherNet stations at Pullman and LIND sites [34].

METRIC Energy Balance Calculation from Satellite Imagery: METRIC is a satellite image processing model that estimates ET as the residual of the surface energy balance [44]. The energy balance can detect the impacts on ET from water shortage, disease, crop variety, planting density, cropping dates, salinity and management practices. A simple form of the surface energy budget equation used in METRIC is the following.

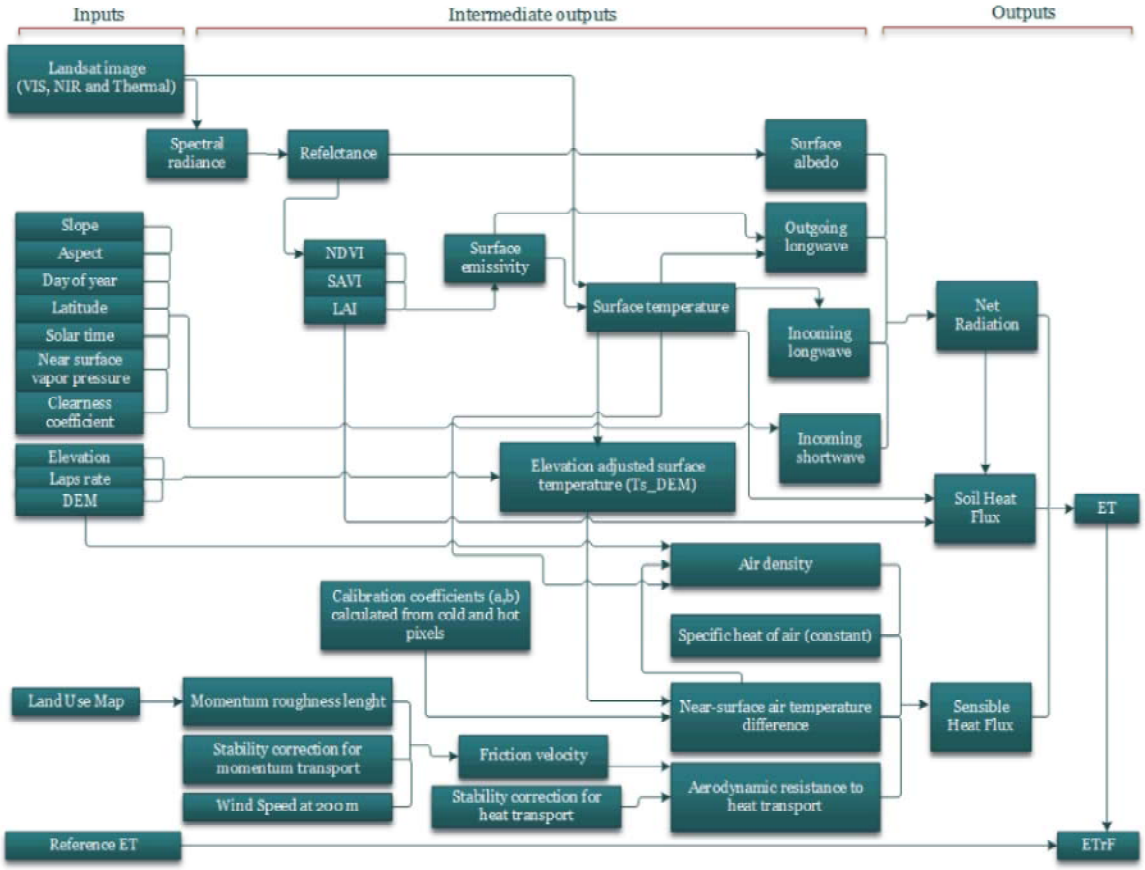

Fig. 2: A brief overview of the METRIC implementation process presenting the inputs, intermediate outputs and final output

$$LE = R_n - H - G \quad (1)$$

where LE is latent heat flux, R_n is net radiation, H is sensible heat flux and G is soil heat flux, all in units of Wm^{-2}. in Wm^{-2}, ET is calculated by dividing latent heat flux by the latent heat of vaporization of water.

Net radiation is the sum of all incoming and outgoing short-wave and long-wave radiation at the surface and is computed from satellite measured narrow-band reflectance and surface temperature (T_s) as described by [45].

$$R_n = R_{s\downarrow} - \propto R_{s\downarrow} + R_{L\downarrow} - R_{L\uparrow} - (1 - \varepsilon_o)\, R_{L\downarrow} \quad (2)$$

Sensible heat flux is the convective heat loss from the surface to the air created by a near-surface temperature gradient. Soil heat flux is the rate of heat conducted into soil and vegetation and is estimated in METRIC from, R_n, T_s and the Normalized Difference Vegetation Index, NDVI [26]. H is estimated in METRIC using a one-dimensional, blended aerodynamic, temperature gradient-based method.

$$H = \rho s_p \frac{dT}{r_{ah}} \quad (3)$$

where ρ is air density (kg/m^3), C_p is air specific heat, (J/kg/K), dT (K) is the temperature difference between two heights (z1 and z2) in a near surface blended layer and r_{ah} is the aerodynamic resistance to heat transport (s/m) between z1 and z2. The use of near surface dT rather than estimates for air and surface temperature, directly, in Equation (3) is done to reduce impacts of bias in temperature, further details about this procedure can be found in [6].

METRIC uses inverse modeling approachto estimate dT for the entire image. This technique in METRIC is called CIMEC (calibrating using inverse modeling at extreme conditions). The calibration is performed using known ET at extreme conditions (cold and hot pixels) in satellite image and biases of all inputs are incorporated into the internal calibration. To determine dT in equation (3) a cold and a hot pixel are selected based on the criteria mentioned by [6]. Briefly, the selection of cold and hot pixels is such that the cold pixel is selected from an

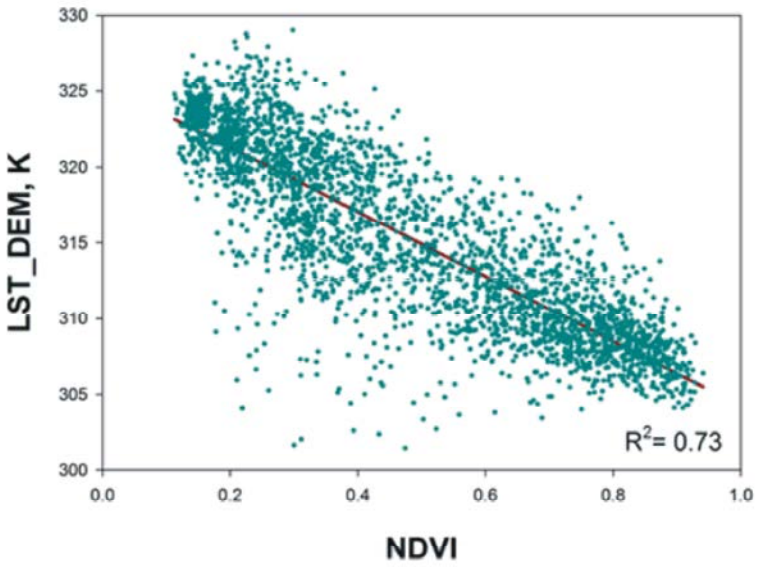

Fig. 3: An example of the relationship of NDVI with LST_DEM (Land Surface Temperature adjusted for elevation, K) for one satellite image in this study. Each point in the image represents a NDVI and LST_DEM value of a sample pixel (30 m). Thousands of sample pixels were picked up as points of interest for calibration sampling in our region of study. This plot isused as aid to select cold and hot pixels; this relationship was plotted for each image during the process of their calibration

agricultural field with a higher NDVI (usually above 0.75), lower T_s (with the assumption that the available energy being used to evapo-transpire water) and an albedo (0.18-0.24) within the range of fully covered agricultural fields. Similarly, hot pixel is assumed to have no ET and is selected from the bare soil with a low NDVI not exceeding 0.2 (usually 0.1-0.15) and a high T_s and albedo within the range of bare agricultural fields (0.17-0.23). Figure 3 plot NDVI vs LST_DEM assist in identifying the range of T_s expected for cold and hot pixels.

The dT associated with a well vegetated pixel (cold pixel) is given as:

$$dT_{cold} = (R_n - G - (0.85 \times Et_r) \times r_{ah} / (\rho \times C_p) \quad (4)$$

Et_r is calculated using weather data using the standardized ASCE Penman-Monteith [46] equation for clipped-grass reference here. Normally for irrigated agriculture alfalfa-based reference is used and to compute the hourly ET for satellite overpass time the ET_r is multiplied by the 1.05. But in dryland region of our study we found out that alfalfa reference and 1.05 constant value was overestimating the cold pixel LE. So we used grass-based ET_r and multiplied that with 0.85 to estimated cold pixel LE in typical settings of our study region (discussed in detail in results section).

A hot pixel is supposed to have zero ET and a large dT value and the value of H can be calculated from R_n and G of that pixel. Sometimes the hot pixel may also have ET especially after a rainfall event, therefore, METRIC used a daily soil water balance and evaporation model that accounts for any residual evaporation from bare soil stemming from antecedent precipitation events [9, 47].

The dT value for hot pixel can be calculated using equation 5.

$$dT_{cold} = H \times r_{ah} / (\rho \times C_p) \quad (5)$$

A linear relationship is assumed to exist between dT and radiometric surface temperature, T_s and the relationship is explained by equation (6). Research by [48], comparisons of final ET estimates over a range of dT values [24, 49] and theoretical arguments [45] suggest that this assumption can apply to a wide range of conditions.

$$dT = aT_s + b \quad (6)$$

where α and b are calibration coefficients that can be found as:

$$a = \frac{dT_{hot} - dT_{cold}}{T_{Shot} - T_{Scold}}, b = dT_{hot} - aT_{shot}$$

T_s is adjusted by delapsing it to a common arbitrary elevation datum, with an image specific lapse rate of 6 K/km [45] to account for changes in T_s caused by warming and cooling of air mass with elevation.

Satellite Data and Preprocessing: Key input data for METRIC are: satellite images, hourly and daily weather data for water balance, land use and land cover image and digital elevation model. Landsat satellite path 43, row 27 covers our study region and Landsat 8 OLI satellite images are used for this research. These images are acquired from USGS EarthExplorer website through the Glovis preview tool. The images downloaded had been preprocessed by USGS EROS using the LPGS preprocessing system resulting in the L1T image product. The images are corrected for radiometric and terrain effects and are georectified as part of the preprocessing. METRIC model is primarily for application with high resolution (30 m) Landsat imagery to achieve ET product that is useful for monitoring water consumption field by field basis. The high-resolution ET is necessary to produce seasonal ET for individual fields as well as for accurate regional ET estimates.

The satellite images with recorded radiations in multiple bands are processed in METRIC to provide NDVI, LAI and surface albedo from visible and near infrared bands and radiometric surface temperature and surface emissivity from mid and thermal infrared bands. These variables are then used to partition the available energy into sensible and latent heat flux components. These surface parameters together with measured field data are used to solve the energy balance, where actual ET is taken as a residual term.

Energy Balance Closure of EC Measurements: An energy balance was conducted to assess the EC flux data quality. Ideally, the energy balance can be closed if both sides in Eq. (7) are accurately quantified [50].

$$(R_n - G) = (H + LE) \quad (7)$$

where R_n (Wm^{-2}) is the net radiation measured by a net radiometer, H and LE (Wm^{-2}) are sensible and latent heat fluxes and G (Wm^{-2}) is soil heat flux.

Half-hourly time series of Rn, H, LE and G over the spring period (March–May, 2013) at CFNT site were analyzed to determine the energy balance closure. This period was selected because there were simultaneous measurements of soil heat flux, soil temperature and soil water content, which allowed for calculating G at the CFNT site. G measurements can affect considerably the energy balance for short timescale but do not influence lambda E values in direct EC measurements [51]. Since G tends to be zero at daily timescale especially in arid climates. Therefore, we also performed energy balance closure on daily time series of Rn, H and LE over the entire measurement period at LIND site in absence of G measurement.

A lack of energy balance closure in turbulent surface heat fluxes measured by EC flux network was revealed in many studies [13, 52, 53]. However, we were unable to find consensus on a single method for forcing energy balance closure (EBC). The closure between footprints of heat flux, H+LE, tends to be less than the available energy (AE) flux, R_n-G. The lack of EBC is normally caused by the non-uniform footprints for components of AE and turbulent heat fluxes as well as instrumental errors and heterogeneous characteristics of landscape. Therefore, it is inappropriate to allocate all errors of EBC to LE and H only because R_N and G can have their own error sources that can significantly affect EBC. The linear regression method to estimate closure error at CFNT site for the three-month period (March, April and May, 2013) shows that the slope and the intercept for the regression of H + LE on R_n-G are 0.83 and 6.00, respectively, with an $R^2$of 0.95.The 83% closure of the energy balance for CFNT is near the average (80%) for good flux measurements using EC methods [54-56]. A portion of the gap in the energy budget at the CFNT site could be accounted for if we had measured the heat storage in the air below the measurement height.

In addition to above, a linear regression between sensible heat flux (H), latent heat flux (LE) and the available energy (R_n) at daily time scale for LIND site was performed considering that G will have minimal effect on energy balance at daily time step [51]. The results of LIND site energy balance closure analysis have satisfactory outcomes presented in Table 2.

Evaluation Period: Four Eddy Covariance flux towers were deployed within a single scene setting of the Landsat 8 path 43 row 27. The remotely sensed ET_a was compared against measured ET at four eddy covariance stations in each image for a total of 26 images. The ET_a was estimated from METRIC for three growing seasons staring from 2013 onward to 2015. The growing season starts from crop emergence and ends at harvest. The CFCT, CFNT and MSMN has crops in all the three growing seasons, with rotations mentioned above and LIND was fallow during 2014 and had WW in 2013 and 2015. Landsat 8 OLI

Table 2: Regression coefficients for 3 years EC data of daily time scale for LIND site

Data (daily time scale)	Intercept (C_o) W/m^2	Coef. On *LE* (C_1)	Coef. On *H* (C_2)	n	R^2	RMSE W/m^2
2013	-9.04	1.07	1.17	365	92	16.68
2014	-3.54	0.98	1.17	365	91	15.74
2015	-10.42	1.12	1.32	365	93	14.52

satellite images were available after every 16 days throughout the growing seasons. But the cloud free images were hard to find at the beginning and end of the growing season. Therefore, those images were cloud masked and then used in spline interpolation for daily ET_a estimates for the entire season.

RESULTS

Energy Balance Closure and Uncertainty Analysis of EC Measurements: The uncertainty in ET measurements from EC due to random errors or gap-filling errors were determined using a Monte Carlo analysis [57] and are reported in Table 3. The annual precipitation was well comparable to the annual ET in view of the dryland agricultural systems.

Evaluation of METRIC: The results of METRIC estimated ET_a and R_n at EC flux foot print scale, was extracted by selecting pixels (30 m each) in the upwind footprint sources area of each EC flux tower site. The EC flux towers footprints were determined using the methodology described by [58] and it was ~100 m for each flux tower. The pixel values of the processed images, for R_n and ET_a at the observation footprint scale from the instantaneous gridded outputs was compared with associated on-site flux measurements. The scatter plot comparison of estimated and measured instantaneous R_n at four sites within the study region is presented in Figure 4. The estimate of instantaneous R_n showed good agreement compared with EC tower measurements at all the four locations within the study region.

R_n is usually considered the most accurate measurement in EC energy flux measurements [50]. The difference in estimated and measured Rn would be because of the uncertainty in the reflected radiances recorded by the satellite due to aerodynamic processes including wind speed, turbulence and buoyancy, all of which are essentially invisible to satellites and impact the transport of vapor and energy fluxes. However the METRIC advantage is that biases inherent to Rn, G and subcomponents of H are essentially cancelled by the subtraction of a bias-canceling estimate for H [18].

The result is an ET map with values ranging between near zero and near ET_r, for images with a range of bare or nearly bare soil and full vegetation cover.

Before going into detailed assessment of the METRIC estimated ET_a a single processed image of ETrF is presented in Figure 5. ETrF is evapotranspiration reference fraction synonymous with the commonly used crop coefficients [59] but it represents actual soil water condition in field and is estimated by dividing ET_a from METRIC with ET_r. ETrF fully capture the spatial trends in water stress, actual vegetation growth conditions or increased ET from intercepted water. The contrast between irrigated and non-irrigated agricultural fields in our study region can easily be understood from Figure 5, the darker green color fields apparently center pivot irrigated are non-water stressed and have higher ETrF and hence ET_a while the dryland agricultural fields are in less dark colors.

The site-specific calibrations for IPNW wheat based non-irrigated cropping system were performed successfully in the current study. The mixed field conditions, steep precipitation gradient and management practices in dryland farming of IPNW were the challenges in calibrating METRIC for this region specifically. Therefore, we have to perform an extensive exercise of model calibrations to come up with a solution for METRIC implementation in IPNW region specific application. The typical changes made were lowering the ETrF value to 0.85 for cold pixel and using clipped grass-based ET_r instead of alfalfa-based ET_r. The grass-based ET_r is helpful in approximation of a near upper limit on ET in drylands, constrained by energy availability. [21, 60] modified METRIC for high soil moisture conditions, [17]suggested that a downward adjustment in ETrF cold from 1.05 is essential for low vegetation or leaf senescence periods especially in high latitudes. As we lowered the ETrF of cold pixel from 1.05 to 0.85 in calibration the implementation produced good results as can be observed from figure 6. METRIC has successfully been able to estimate ET fairly accurately. In the statistical analysis of estimated and measured ET the coefficient of determination has always been above 0.85 and SEE below 0.5 that indicates the strength of METRIC model in estimating regional ET_a. The study region has three precipitation zones with annual precipitation ranging from 250mm to 650mm (Figure 1). And the variation in SEE from high precipitation to low precipitation site is 0.48 to 0.31 which is not much significant keeping in view a 400mm annual precipitation difference between those two sites.

Table 3: Annual and seasonal evapotranspiration (ET) and precipitation and the associated uncertainties at each site during the measurement period

Site-year (Crop)*			ET (mm)	Precipitation (mm)
MSMN	2013 (SB)	Annual	506 (±2)	584
		MGS	237 (±1)	77
		oMGS	269 (±2)	507
	2014 (Pea)	Annual	501 (±2)	536
		MGS	227 (±1)	43
		oMGS	274 (±2)	493
CAF-NT	2012 (WW)	Annual	615(±3)	515
		MGS	433 (±2)	156
		oMGS	182 (±2)	359
	2013 (SG)	Annual	428 (±2)	539
		MGS	258 (±2)	85
		oMGS	170 (±2)	454
	2014 (WW)	Annual	510(±3)	455
		MGS	349 (±1)	111
		oMGS	161 (±2)	344
CAF-CT	2013 (SG)	Annual	421 (±2)	539
		MGS	215 (±2)	85
		oMGS	206 (±1)	454
	2014 (WW)	Annual	507(±3)	455
		MGS	348 (±2)	111
		oMGS	159 (±2)	344
LIND†	2012	Annual	219 (±3)	250
	2013 (WW)	Annual	375(±3)	272
		MGS	265 (±2)	85
		oMGS	110 (±2)	187
	2014	Annual	175 (±4)	175

*Abbreviations: SB-spring barley, WW-winter wheat and SG-spring garbanzo.

†LIND was fallow during the crop year of 2012 and 2014, so no MGS was defined for these two years.

Table 4: Statistical comparison of estimated and measured instantaneous net radiation (W m^{-2})

	R_n(Instantaneous)		
Study site	SEE	BIAS	R^2
CFNT	34.28	-11.7	86
CFCT	25.41	-8.4	94
LIND	23	2.5	92
MSMN	17.32	2.7	97

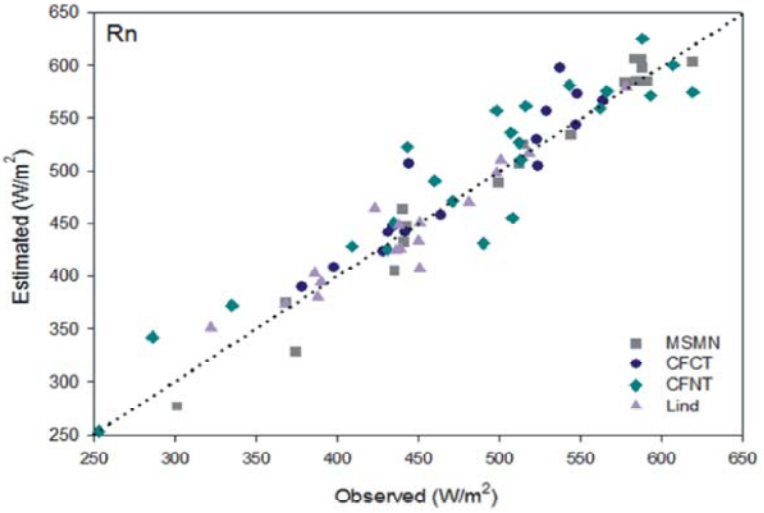

Fig. 4: Scatter plot comparison of measured with estimated instantaneous net radiation

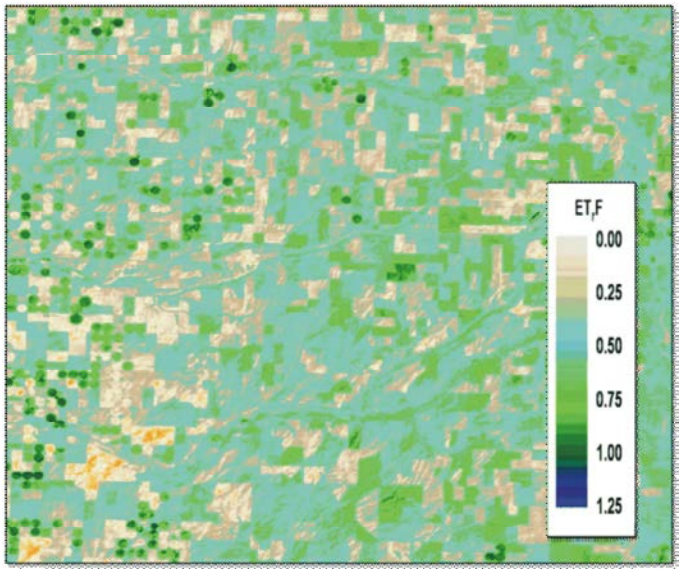

Fig. 5: ETrF image showing the contrast between irrigated fields ET and non-irrigated fields ET at larger scale

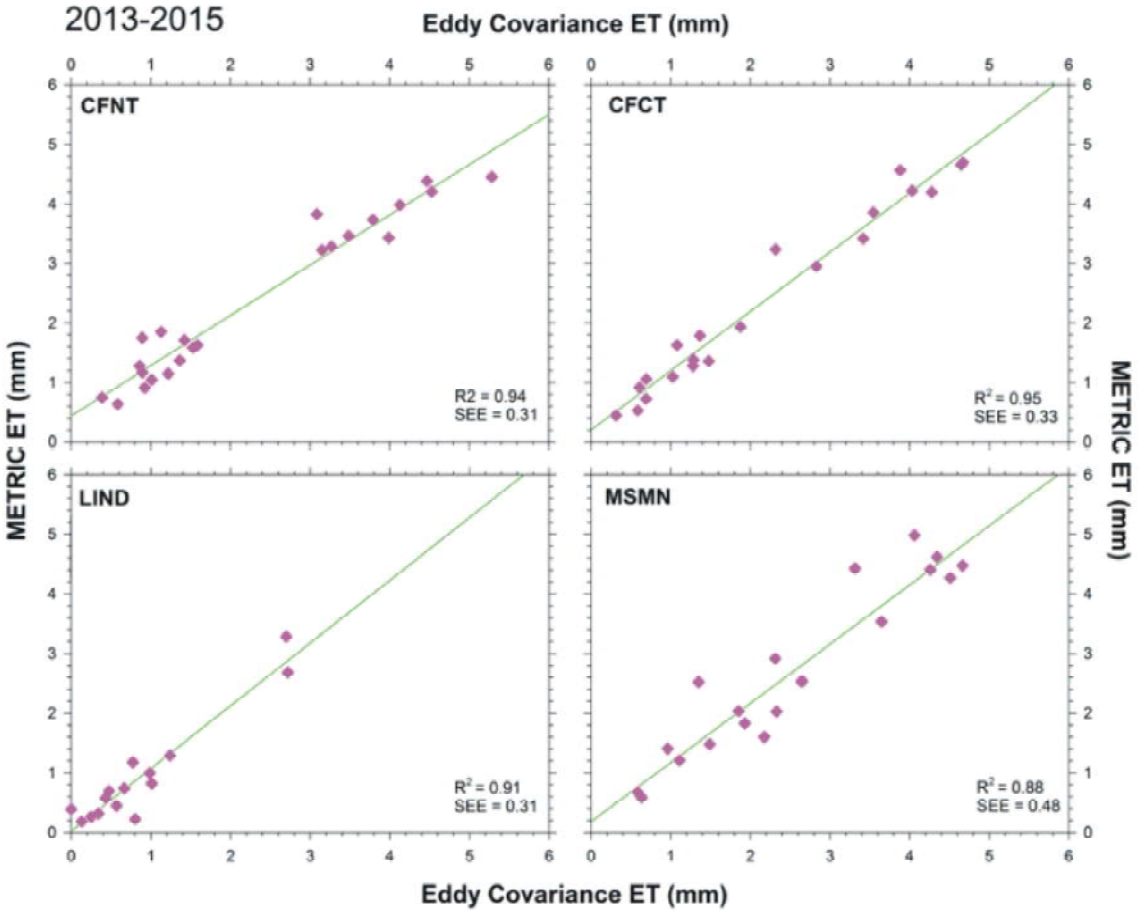

Fig. 6: ET (mm day^{-1}) comparison between eddy covariance measurements and METRIC estimate for satellite overpass dates

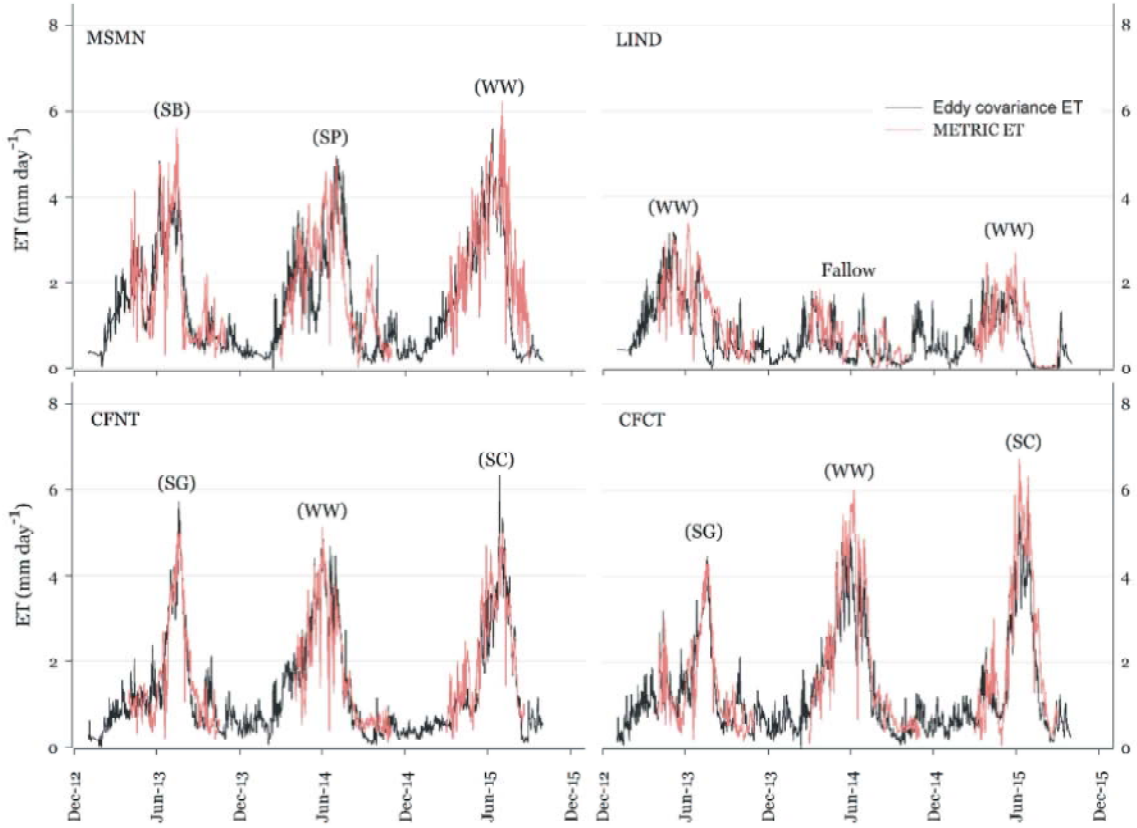

Fig. 7: Seasonal ET comparison between METRIC estimate and eddy covariance measurements for all the four sites and three growing seasons in our study region. The abbreviations on each seasonal curve shows the crop on ground there. Abbreviations: SB-spring beans, SP-spring peas, WW-winter wheat, SG-spring garbanzo and SC-spring canola

Table 5: Statistical analysis of seasonal ET estimates from METRIC and eddy covariance measurement. Abbreviations: SEE-standard error of the estimate, R^2-coefficient of determination and R-Pearson's correlation coefficient

Site	Years	SEE(mm day^{-1})	R2	R
CFNT	2013	0.56	0.78	0.89
	2014	0.46	0.86	0.93
	2015	0.50	0.85	0.92
CFCT	2013	0.56	0.70	0.83
	2014	0.57	0.88	0.94
	2015	0.73	0.84	0.92
MSMN	2013	0.73	0.70	0.83
	2014	0.87	0.47	0.69
	2015	0.82	0.61	0.78
LIND	2013	0.65	0.36	0.60
	2014	0.35	0.31	0.55
	2015	0.47	0.54	0.74

We estimated seasonal ET_a based on the daily estimates from satellite overpass time using cubic spline interpolation between images [45]. The cubic spline interpolation is performed primarily on cloud free ETrF images. The output of seasonal ETrF estimates resembles K_C(crop-coefficient [9]) curve, which after multiplication with seasonal ET_r can produce estimates of seasonal ET_a. The comparison of EC ET measurements and seasonal estimates of ET for the three growing seasons in 2013, 2014 and 2015 at all the four sites in our study region are presented in Figure 7. Generally, the differences between estimated and observed can be because of error in EC flux measurements as well as biases in ET_a estimation by METRIC. Overall the cubic spline interpolation has performed well to produce these estimates as the Pearson's correlation coefficient (R) is positive and has value above 0.90 for CFCT CFNT and a little lower value for MSMN and LIND (Table 5). The coefficient of determination for the analysis of ET on satellite overpass dates was significantly higher (Figure 6) than the same for seasonal estimates especially for LIND site. This means that the biases in seasonal ET interpolated from satellite overpass dates can be due to residual evaporation from antecedent precipitation and uncertainty due to cloud

filled images. For MSMN and LIND sites It can be observed from Figure 7 that the estimated and measured ET agreed well during peak growing season (May-July) however the curves did not match well at the start and the end of the season. This bias may be because of two reasons, one as explained the uncertainty due to cloud-filling and the other may be because using the average seasonal wind direction to select the pixel for comparison with EC measurements. Since most of the precipitation is received at the start and after the end of growing season (Table 3) therefore during this time of the season most of the images processed were cloudy and they were cloud masked and used in spline interpolation.

The LIND station has arid climate and 50% less precipitation than that recorded at CFNT/CFCT, in addition to that WW residue is left on field in LIND to conserve soil moisture. This practice may have introduced a bias in our image such that the soil evaporation assigned from soil water balance model to the hot pixel may have not been present actually in field, since the bias is positive as well. The accuracy of ET estimates for different crops on ground with variable annual precipitation for all the four sites reveals that METRIC can estimate regional ET without the information about what crop is on ground and soil-water conditions.

METRIC has some significant advantages over conventional methods of estimating ET from crop coefficient curves in that neither crop development stages nor the specific crop type needs to be known with METRIC. This study presented good example of site-specific METRIC implementation that may be required to improve accuracy of estimates of ET from natural systems and illustrate the value of specific knowledge of native systems, principles of aerodynamic transfer and boundary layer development, soil physics and energy transfer limitations.

SUMMARY AND CONCLUSIONS

We estimated actual ET from typical dryland farming in Washington State for three consecutive growing seasons, 2013 onwards by implementing METRIC (a surface energy balance algorithm) with satellite imagery. The actual ET was estimated as the residual of the surface energy balance. R_n is computed by subtracting all the outgoing radiant fluxes from all incoming radiant fluxes, G is determined from empirical relationship and is normally a small percentage of R_n. For H, a linear relationship between the near surface temperature gradient (dT) and the surface temperature (Ts) is developed in METRIC by employing the Calibration using Inverse Modeling at Extreme Conditions (CIMEC). The use of the CIMEC process excludes the effect of potential biases related to energy balance components, radiometric correction on the final estimated ET. The calibration at hydrological extremes identified by land surface temperature (LST) within the particular land use category of the image is important because LST quickly senses water stress in crops than other indicators like vegetation indices and it rapidly reflects the water stress conditions by an increase in temperature.

For results verification we had four flux towers deployed over 100 miles within a single scene setting of the Landsat8 satellite path 43 row 27. The remotely sensed ET was compared against the flux towers' observed ET through eddy covariance, a most sophisticated and accurate method to observe ET. Estimated and observed ET showed a good argument. The RMSE was also encouragingly low and the Nash-Sutcliffe Efficiency Coefficient showed that METIRC was 82-98% efficient in estimating actual ET. However, this study employed some modifications in METRIC model implementation, including a decrease in ETrF value for cold anchor pixel and use of clipped grass instead of alfalfa in standard reference ET from Penman Monteith method for typical drylands setting of Washington State. This study is unique because it used different boundary conditions in METRIC for its implementation in dryland regions to estimate ET fairly accurately in water stressed and mixed field conditions at large scale and the results are reliable because they were compared against the most accurate ground observations at four points within a single image domain. This study provided solution for ET estimation under water stressed conditions with high accuracy at regional scale. This information can be used to develop water budgets, to monitor drought and to estimate agricultural water use for water managers and irrigation engineers in order to make informed decisions regarding water resource management.

However, METRIC requires trained experts who possess a strong background in energy balance and radiation physics and an adequate knowledge of vegetation characteristics. It also requires high quality hourly time scale data.

It is important to know the type of setting for which ET estimates are intended and the conditions from which the measurements are made. The precise determination of large scale ET is a challenge and has important practical significance in climate change studies, water resource planning and management, agricultural water-saving, crop

production and environmental issues. Large scale ET information can be used in cropping system models for real time yield estimates and for decision support. Remote sensing (RS) especially from satellites has the ability to capture the actual field conditions and RS observations used with surface energy balance algorithms can provide widespread spatio-temporal actual ET estimates.

REFERENCES

1. Glenn, E.P., *et al*., 2007. Integrating Remote Sensing and Ground Methods to Estimate Evapotranspiration. Critical Reviews in Plant Sciences, 26(3): 139-168.
2. Bastiaanssen, W.G.M., *et al*., 2012. Surface energy balance and actual evapotranspiration of the transboundary Indus Basin estimated from satellite measurements and the ETLook model. Water Resources Research, 48(11): n/a-n/a.
3. Tian, F., *et al*., 2013. Estimation of evapotranspiration and its partition based on an extended three-temperature model and MODIS products. Journal of Hydrology, 498: 210-220.
4. Singh, R., A. Irmak, S. Irmak and D. Martin, 2018. Application of SEBAL Model for Mapping Evapotranspiration and Estimating Surface Energy Fluxes in South-Central Nebraska. Journal of Irrigation and Drainage Engineering, 134(3): 273-285.
5. Teixeira, A.H.D.C., *et al*., 2009. Reviewing SEBAL input parameters for assessing evapotranspiration and water productivity for the Low-Middle São Francisco River basin, Brazil: Part A: Calibration and validation. Agricultural and Forest Meteorology, 149(3–4): 462-476.
6. Allen, R., *et al*., 2005. METRIC: High Resolution Satellite Quantification of Evapotranspiration.
7. Kalma, J.D., T.R. McVicar and M.F. McCabe, 2008. Estimating Land Surface Evaporation: A Review of Methods Using Remotely Sensed Surface Temperature Data. Surveys in Geophysics, 29(4): 421-469.
8. Bastiaanssen, W.G.M., D.J. Molden and I.W. Makin, 2000. Remote sensing for irrigated agriculture: examples from research and possible applications. Agricultural Water Management, 46(2): 137-155.
9. Allen, R.G., *et al*., 1998. Crop evapotranspiration-Guidelines for computing crop water requirements-FAO Irrigation and drainage paper 56. FAO, Rome, 300(9): D05109.
10. Senay, G.B., M.E. Budde and J.P. Verdin, 2011. Enhancing the Simplified Surface Energy Balance (SSEB) approach for estimating landscape ET: Validation with the METRIC model. Agricultural Water Management, 98(4): 606-618.
11. Yang, X., *et al*., 2013. Estimation of Daily Actual Evapotranspiration from ETM+ and MODIS Data of the Headwaters of the West Liaohe Basin in the Semiarid Regions of China. Journal of Hydrologic Engineering, 18(11): 1530-1538.
12. Jia, L., *et al*., 2009. Regional estimation of daily to annual regional evapotranspiration with MODIS data in the Yellow River Delta wetland. Hydrol. Earth Syst. Sci., 13(10): 1775-1787.
13. Hwang, K. and M. Choi, 2013. Seasonal trends of satellite-based evapotranspiration algorithms over a complex ecosystem in East Asia. Remote Sensing of Environment, 137: 244-263.
14. Byun, K., U.W. Liaqat and M. Choi, 2014. Dual-model approaches for evapotranspiration analyses over homo- and heterogeneous land surface conditions. Agricultural and Forest Meteorology, 197: 169-187.
15. Chirouze, J., *et al*., 2014. Intercomparison of four remote-sensing-based energy balance methods to retrieve surface evapotranspiration and water stress of irrigated fields in semi-arid climate. Hydrol. Earth Syst. Sci., 18(3): 1165-1188.
16. Choi, M., *et al*., 2009. An intercomparison of three remote sensing-based surface energy balance algorithms over a corn and soybean production region (Iowa, U.S.) during SMACEX. Agricultural and Forest Meteorology, 149(12): 2082-2097.
17. Liaqat, U.W. and M. Choi, 2015. Surface energy fluxes in the Northeast Asia ecosystem: SEBS and METRIC models using Landsat satellite images. Agricultural and Forest Meteorology, 214-215: 60-79.
18. Mkhwanazi, M., J.L. Chávez and E.H. Rambikur, 2012. Comparison of large aperture scintillometer and satellite-based energy balance models in sensible heat flux and crop evapotranspiration determination. International journal of Remote Sensing Applications, 1: 24-30.
19. Paço, T.A., *et al*., 2014. Evapotranspiration and crop coefficients for a super intensive olive orchard. An application of SIMDualKc and METRIC models using ground and satellite observations. Journal of Hydrology, 519, Part B: pp: 2067-2080.

20. Morton, C.G., *et al*., 2013. Assessing Calibration Uncertainty and Automation for Estimating Evapotranspiration from Agricultural Areas Using METRIC. JAWRA Journal of the American Water Resources Association, 49(3): 549-562.
21. Singh, R.K. and A. Irmak, 2011. Treatment of anchor pixels in the METRIC model for improved estimation of sensible and latent heat fluxes. Hydrological Sciences Journal, 56(5): 895-906.
22. Trezza, R., R. Allen and M. Tasumi, 2013. Estimation of Actual Evapotranspiration along the Middle Rio Grande of New Mexico Using MODIS and Landsat Imagery with the METRIC Model. Remote Sensing, 5(10): 5397.
23. Singh, R., A. Irmak, S. Irmak, and D. Martin, 2007. Satellite-Based Energy Balance for Mapping Evapotranspiration with Internalized Calibration (METRIC)-Model. Journal of Irrigation and Drainage Engineering, 133(4): 380-394.
24. Allen, R.G., *et al*., 2007. Satellite-based energy balance for mapping evapotranspiration with internalized calibration (METRIC) Applications. Journal of Irrigation and Drainage Engineering, 133(4): 395-406.
25. Allen, R., *et al*., 2012. METRIC Mapping Evapotranspiration at High Resolution. Applications Manual for Landsat Satellite Imagery. Version, 2(8).
26. Allen, R., *et al*., 2011. Satellite-based ET estimation in agriculture using SEBAL and METRIC. Hydrological Processes, 25(26): 4011-4027.
27. Stöckle, C., *et al*., 2012. Carbon storage and nitrous oxide emissions of cropping systems in eastern Washington: A simulation study. Journal of Soil and Water Conservation, 67(5): 365-377.
28. Brown, T. and D. Huggins, 2012. Soil carbon sequestration in the dryland cropping region of the Pacific Northwest. Journal of Soil and Water Conservation, 67(5): 406-415.
29. Papendick, R., *et al*., *Description of the region.* Crop residue management to reduce erosion and improve soil quality. USDA-ARS Conserv. Res. Rep, 1995. 40: p. 4-9.
30. Schillinger, W.F., *et al*., 2006. Dryland cropping in the Western United States, in Agronomy Monograph No. 23. 2006, American Society of Agronomy: Madison, pp: 365-393.
31. Purakayastha, T., D. Huggins and J. Smith, 2008. Carbon sequestration in native prairie, perennial grass, no-till and cultivated Palouse silt loam. Soil Science Society of America Journal, 72(2): 534-540.
32. NOAA, National Climate Data Center, {*http://www.ncdc.noaa.gov/}*. 2015.
33. Al-Mulla, Y.A., *et al*., 2009. Soil Water and Temperature in Chemical Versus Reduced-Tillage Fallow in a Mediterranean Climate. Applied Engineering in Agriculture, 25(1): 45-54.
34. Ag Weather Net, Washington State University.{*http://weather.wsu.edu/awn.php}*. 2014.
35. Chi, J., *et al*., 2016. Assessing carbon and water dynamics of no-till and conventional tillage cropping systems in the inland Pacific Northwest US using the eddy covariance method. Agricultural and Forest Meteorology, 218: 37-49.
36. Waldo, S., *et al*., 2016. Assessing carbon dynamics at high and low rainfall agricultural sites in the inland Pacific Northwest US using the eddy covariance method. Agricultural and Forest Meteorology, 218: 25-36.
37. Kaimal, J.C. and J.J. Finnigan, 1994. Atmospheric boundary layer flows: their structure and measurement. Oxford University Press.
38. Moncrieff, J.B., *et al*., 1997. A system to measure surface fluxes of momentum, sensible heat, water vapour and carbon dioxide. Journal of Hydrology, 188: 589-611.
39. Moncrieff, J., *et al*., 2004. Averaging, detrending and filtering of eddy covariance time series, in Handbook of Micrometeorology. Springer, pp: 7-31.
40. Webb, E.K., G.I. Pearman and R. Leuning, 1980. Correction of flux measurements for density effects due to heat and water vapour transfer. Quarterly Journal of the Royal Meteorological Society, 106(447): 85-100.
41. Papale, D., *et al*., 2006. Towards a standardized processing of Net Ecosystem Exchange measured with eddy covariance technique: algorithms and uncertainty estimation. Biogeosciences, 3(4): 571-583.
42. Falge, E., *et al*., 2001. Gap filling strategies for defensible annual sums of net ecosystem exchange. Agricultural and Forest Meteorology, 107(1): 43-69.
43. Moffat, A.M., *et al*., 2007. Comprehensive comparison of gap-filling techniques for eddy covariance net carbon fluxes. Agricultural and Forest Meteorology, 147(3): 209-232.
44. Allen, R.G., *et al*., 2002. Evapotranspiration from a satellite-based surface energy balance for the Snake Plain Aquifer in Idaho. US Committee on Irrigation and Drainage: Denver, pp: 167-178.

45. Allen, R.G., M. Tasumi and R. Trezza, 2007. Satellite-based energy balance for mapping evapotranspiration with internalized calibration (METRIC) Model. Journal of Irrigation and Drainage Engineering, 133(4): 380-394.
46. ASCE-EWRI, 2005. The ASCE standardized reference evapotranspiration equation: ASCE-EWRI Standardization of Reference Evapotranspiration Task Committe Report. ASCE Reston.
47. Allen, R.G., 2011. Skin layer evaporation to account for small precipitation events—An enhancement to the FAO-56 evaporation model. Agricultural Water Management, 99(1): 8-18.
48. Bastiaanssen, W.G.M., 1995. Regionalization of surface flux densities and moisture indicators in composite terrain; a remote sensing approach under clear skies in mediterranean climates. 1995, Wageningen, SC-DLO, 1995. Report 109, pp: 271.
49. Tasumi, M., *et al*., 2005. Satellite-Based Energy Balance to Assess Within-Population Variance of Crop Coefficient Curves. Journal of Irrigation and Drainage Engineering, 131(1): 94-109.
50. Allen, R., 2008. Quality Assessment of Weather Data and Micrometeological Flux
—Impacts on Evapotranspiration Calculation. Journal of Agricultural Meteorology, 64(4): 191-204.
51. Teixeira, C., A.H. and W.G.M. Bastiaanssen, 2010. Five methods to interpret field measurements of energy fluxes over a micro-sprinkler-irrigated mango orchard. Irrigation Science, 30(1): 13-28.
52. Ershadi, A., *et al*., 2014. Multi-site evaluation of terrestrial evaporation models using FLUXNET data. Agricultural and Forest Meteorology, 187: 46-61.
53. Tang, R., *et al*., 2013. Evaluating one- and two-source energy balance models in estimating surface evapotranspiration from Landsat-derived surface temperature and field measurements. International Journal of Remote Sensing, 34(9-10): 3299-3313.
54. Foken, T., 2008. The Energy Balance Closure Problem: an Overview. Ecological Applications, 18(6): 1351-1367.
55. Twine, T.E., *et al*., 2000. Correcting eddy-covariance flux underestimates over a grassland. Agricultural and Forest Meteorology, 103(3): 279-300.
56. Wilson, K., *et al*., 2002. Energy balance closure at FLUXNET sites. Agricultural and Forest Meteorology, 113(1): 223-243.
57. Richardson, A.D. and D.Y. Hollinger, 2007. A method to estimate the additional uncertainty in gap-filled NEE resulting from long gaps in the CO2 flux record. Agricultural and Forest Meteorology, 147(3-4): 199-208.
58. Kljun, N., *et al*., 2004. A simple parameterisation for flux footprint predictions. Boundary-Layer Meteorology, 112(3): 503-523.
59. Allen, R.G., *et al*., 2013. Automated Calibration of the METRIC-Landsat Evapotranspiration Process. JAWRA Journal of the American Water Resources Association, 49(3): 563-576.
60. Singh, R.K., *et al*., 2011. Estimating seasonal evapotranspiration from temporal satellite images. Irrigation Science, 30(4): 303-313.